5-2016

Extending the Supermassive Black Hole Mass-Pitch Angle Relation to Moderate Redshifts

Logan H. Jones
University of Arkansas, Fayetteville

EXTENDING THE SUPERMASSIVE BLACK HOLE MASS-PITCH ANGLE RELATION TO MODERATE REDSHIFTS

Logan Jones
Department of Physics, University of Arkansas
Fayetteville, AR 72701

ABSTRACT

I extend the empirical correlation between central supermassive black hole mass M and spiral arm pitch angle P in spiral galaxies to intermediate redshifts using a sample of 14 type 1 Seyfert galaxies. Nuclear black hole masses are measured from the widths and luminosities of the broad Hβ and MgII emission lines, and pitch angles are measured using two independent image analysis techniques. I find the best-fit relation $\log(M/M_{\odot}) = (8.31 \pm 0.28) - (0.058 \pm 0.016)P$, which indicates little to no evolution compared to the published M-P relation for local spirals.

1. INTRODUCTION

One of the greatest astronomical developments of the past 50 years has been the discovery of supermassive black holes (SMBHs) hiding in the centers of nearly all massive galaxies, including those hosting quasars and other active nuclei. Prior to the 1960s, black holes were largely considered a mathematical curiosity, artifacts that fall out of the Schwarzchild and Kerr metrics in Einstein's general theory of relativity. Their theoretical utility was demonstrated in the works of Lynden-Bell (1969), Lynden-Bell & Rees (1971), and Rees (1984), among others; evidence for their physical reality was soon to follow. See Graham (2016), Kormendy & Gebhardt (2001), and references therein for a more thorough account of the observational history of SMBHs. As evidence continues to mount for the existence of SMBHs in galactic nuclei, the ability to reliably measure black hole masses is crucial to our understanding of the coevolution of these objects and their host galaxies.

1.1. *Black Hole Mass Measurements*

Kormendy & Gebhardt (2001) detail the first efforts to measure SMBH masses in the Milky Way and nearby galaxies. Ground- and space-based observations of stellar and gas kinematics around the central mass, as well as H_2O maser emission diagnostics, have provided mass estimates for ~37 SMBHs in the range 10^6 to 10^8 $M_{\odot}$ (Kormendy & Gebhardt 2001). Peterson et al. (2004) summarize an additional measurement technique, known as reverberation mapping, which was employed for the ~35 active galaxies described in that paper (more on reverberation mapping in section 1.2). While direct and therefore preferable, these techniques are not feasible for building up a statistically large sample of SMBH masses because they are observationally demanding or even impossible with current instruments, especially for more distant galaxies. Peterson & Horne (2004), for example, recommend 150-200 nights of spectroscopic observations to produce high-quality reverberation maps for any individual nucleus.

A web of correlations between broader properties of a galaxy has also given rise to a variety of indirect mass measurement techniques. Most of these relate SMBH mass M_{BH} to more readily-measurable properties of the host galaxy or its bulge, including bulge/spheroid luminosity L_{sph} and bulge/spheroid mass M_{sph} (see, for example, Magorrian et al. 1998 and Kormendy & Gebhardt 2001); Sérsic index n, which traces the stellar mass concentration in the bulge (Graham

& Driver 2007); and velocity dispersion σ_* of bulge stars (Ferrarese & Merritt 2000; Gebhardt et al. 2000). The M-σ_* relation became especially notable for its apparently low intrinsic scatter, though it is not without its controversies. There remains considerable debate over the true slope of the best-fit power law (stemming from both sample selection effects and different statistical methodologies, as described in Graham 2016) and its applicability to spiral galaxies, where disk and bar stars can contaminate measurements of σ_*.

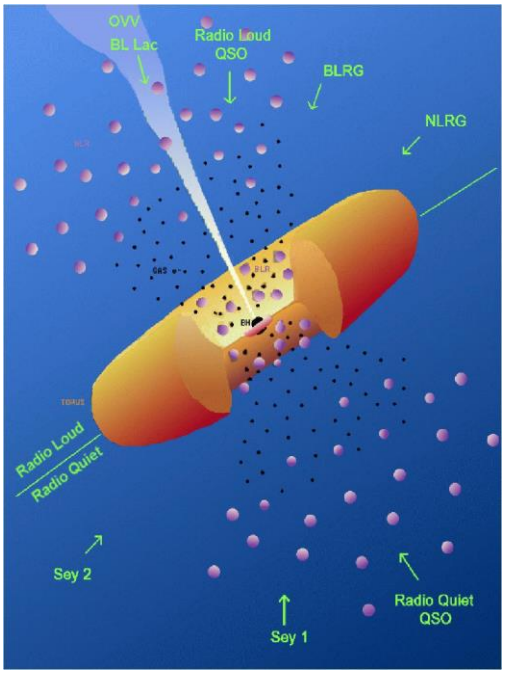

Fig. 1. — Illustration of the basic structure of AGN (not to scale). Image credit to Southampton Gamma-ray Astrophysics Group; originally printed in Urry & Padovani 1995.

1.2. *Active Galactic Nuclei*

Another major development of the past half-century has been the discovery and characterization of radio-loud and radio-quiet quasars, Seyfert galaxies, and other classes of objects that are collectively referred to as active galactic nuclei (AGN). Although AGN properties vary widely from class to class, AGN are known to generate enormous amounts of radiative energy in a compact region of space and are often as luminous as the entire host galaxy. Ferrarese & Ford (2005) give a short but thorough summary of the observational histories of AGN and the development of the current paradigm of AGN activity: accretion of gas and dust onto a nuclear SMBH, surrounded by a thick, dusty torus. The general structure of an AGN is shown in Fig. 1. Hot gas and dust emits blackbody-like radiation across the continuum as it accretes onto the central SMBH. This emission is partly reprocessed by rapidly-orbiting clouds in the broad line region (BLR), so called because of Doppler-broadening of emission lines, and partly by the slower-moving clouds in the narrow line region (NLR). Some obscuration also occurs due to a torus of molecular gas and dust extending beyond the NLR. The resulting spectral energy distribution generally includes a continuum component, roughly modeled within some wavelength range by a single power law, and numerous emission and absorption features. Under proposed unified models of active galactic nuclei, classification of an AGN depends strongly on its orientation relative to the observer (Antonucci 1993; Urry & Padovani 1995; Kazanas et al. 2012). Type 1 Seyfert galaxies, which are the focus of this paper, are viewed at intermediate angles such that much of the BLR emission remains unobscured. They are typically radio quiet and are characterized by the presence of both broad (full width at half maximum FWHM > 500 km s^{-1}) and narrow emission lines (FWHM < 500 km s^{-1}). Type 2 Seyfert galaxies have the same general properties as type 1s but are oriented such that the dusty tori are viewed nearly edge-on, obscuring the BLR and leaving only narrow emission lines in their spectra. Intermediate classifications, like Seyfert types 1.5 and 1.9, have also been proposed to describe galaxies with relatively weak broad lines.

The extreme luminosities of AGN-hosting galaxies allow them to be observed at much higher redshifts than their inactive counterparts, at the cost of obscuring a number of observable features that could be useful in determining the mass of the central black hole. There remains some debate, for example, whether active and inactive galaxies follow different M-σ_* relations, partly due

to the increased difficulty of obtaining reliable measurements of bulge star spectral features in the glow of an AGN (e.g., Woo 2013).

1.3. *The M-P Relation*

One property of a spiral galaxy whose measurability is typically not affected by the presence of an active nucleus is the spiral arm pitch angle. Modal density wave theory (e.g., Shu 1984 and Lin & Shu 1964), one of the leading theories of spiral structure, predicts a correlation between a disk galaxy's central mass and the pitch angle P of its spiral arms, which quantifies the "tightness" of the spiral pattern. Such a relationship was first reported by Seigar et al. (2008) for a sample of 27 low-redshift spiral galaxies as

$$\log(M/M_{\odot}) = (8.44 \pm 0.10) - (0.076 \pm 0.05)P$$

for SMBHs between $10^5 M_{\odot}$ and $10^8 M_{\odot}$. This was refined by Berrier et al. (2013) using a sample of 34 low-z galaxies, who found the relation

$$\log(M/M_{\odot}) = (8.21 \pm 0.16) - (0.062 \pm 0.009)P \qquad (1)$$

over approximately the same range of M. This result is consistent with both the density wave theory and the manifold theory of spiral structure (e.g., Romero-Gómez et al. 2006), though exploring which theory is to be preferred is beyond the scope of this paper. See the introduction and appendix of Berrier et al. (2013) for more on the theoretical foundations of the *M-P* relation in the context of density wave theory.

Since measurement of pitch angle requires only an image of a galaxy, the *M-P* relation as a method for estimating SMBH masses has numbers on its side, compared to spectroscopy-based methods. Large quantities of high-quality archival imaging data potentially allow for a substantial number of SMBH mass estimates to be made for spiral galaxies across a broad range of redshifts, which can be put to use in various astronomical endeavors – for example, in determining a black hole mass function for disk galaxies (Davis et al. 2014). However, the *M-P* relation given in (1) was found using relatively nearby galaxies only, with redshifts $z < 0.04$. In order for the *M-P* relation to be maximally useful, it must be explored at increasingly higher z and tested for evolution in its mathematical form.

In this paper, I present the results of independent measurement of SMBH masses and spiral arm pitch angles in a sample of type 1 AGN-hosting galaxies in the redshift range $0.2 < z < 1.4$. This work is part of a broader collaborative effort to expand upon the work of Berrier et al. (2013) and extrapolate the *M-P* relation to higher redshifts. The structure of the paper is as follows: in section 2, I will describe the spectroscopic and imaging data used in this work along with methods for determining SMBH mass and pitch angle. I correlate the measured quantities in section 3, and discuss the implications and caveats of these results in section 4.

In this work I assume a flat ΛCDM cosmology with $H_0 = 69.6$ km s^{-1} Mpc^{-1}, $\Omega_{\Lambda} = 0.714$, and $\Omega_{\mathrm{M}} = 0.286$, based on the analysis of combined WMAP9+SPT+ACT+BAO+H0 data by Bennett et al. (2014).

TABLE 1
Sample Information

Galaxy	Redshift	Source	Scaling Relation	$\log[M_{BH}/M_{\odot}]$	P (deg.)	Preferred
XMMC 5121	0.196	1	Hβ	7.58 ± 0.08	9.53 ± 1.41	2DFFT
XMMC 2016	0.345	1	Hβ	7.87 ± 0.07	26.79 ± 4.03	2DFFT
XMMC 35	0.346	1,4*	Hβ	6.66 ± 0.07	31.61 ± 1.38	2DFFT
XMMC 5261	0.376	1	Hβ	7.65 ± 0.09	5.75 ± 0.76	2DFFT
XMMC 164	0.529	1	Hβ	7.45 ± 0.09	12.80 ± 2.22	2DFFT
XMMC 22	0.554	1	Hβ,MgII	7.23 ± 0.10	25.60 ± 2.68	2DFFT
XMMC 2234	0.692	3*,4	Hβ	5.87 ± 0.25	13.92 ± 5.04	Spirality
XMMC 61	0.728	3	Hβ	6.50 ± 0.14	7.51 ± 3.39	—
XMMC 141	0.832	2	MgII	7.87 ± 0.15	20.28 ± 3.58	2DFFT
XMMC 39	0.851	2	MgII	7.60 ± 0.15	12.59 ± 2.92	2DFFT
XMMC 2653	0.946	2	MgII	7.67 ± 0.09	12.34 ± 3.56	2DFFT
XMMC 47	0.959	2	MgII	7.81 ± 0.06	18.16 ± 3.65	2DFFT
XMMC 5523	1.087	3	MgII	8.06 ± 0.10	9.61 ± 3.39	Spirality
XMMC 56	1.407	4	MgII	7.82 ± 0.07	10.59 ± 8.87	Spirality

NOTE — Column 1: galaxy XMM-COSMOS designation. Column 2: galaxy redshift. Column 3: sources of spectra, with preferred sources starred. Column 4: emission line(s) used to estimate M_{BH}. Column 5: logarithm of measured black hole mass. Column 6: measured (absolute) pitch angle. Column 7: preferred pitch angle measurement technique. **References**: (1) Alam et al. 2015; (2) Prescott et al. 2006; (3) Lilly et al. 2007; (4) Trump et al. 2009.

2. SAMPLE AND METHODS

My sample is drawn from that of Lusso et al. (2010), who consider 545 type 1 AGN selected on the basis of their X-ray luminosities, 327 of which had available spectroscopic data. Of these 327, 19 had visible apparent spiral structure when inspected by eye. One of these galaxies was later discovered to contain dual AGNs, with the merger's tidal tail forming the apparent spiral pattern, and excluded from the sample. Four others were also excluded for one or more of the following reasons: (1) their spectra showed no broad lines or were unable to be viewed for analysis; (2) their angular size in pixels was too small for reliable measurement of pitch angle; or (3) their identification as spiral galaxies was too questionable to warrant inclusion in this paper. This leaves a sample of 14 type 1 AGN-hosting spirals in the redshift range $0.196 < z < 1.407$.

2.1. *Measuring M_{BH}*

A total of sixteen spectra were used to measure SMBH mass, since two objects in my sample had spectra available from multiple sources, as noted column 3 of Table 1. Six spectra come from the Sloan Digital Sky Survey (SDSS) 2.5 m telescope at Apache Point Observatory using the Sloan *g*-band filter; four come from the Hectospec instrument on the MMT 6.5 m telescope; three come from the IMACS instrument on the 6.5 m Magellan/Baade telescope in the wavelength range 5600-9200 Å; three come from the zCOSMOS survey of Lilly et al. 2007 and cover the wavelength range 5500-9500 Å. See Alam et al. (2015), Prescott et al. (2006), Lilly et al. (2007), Trump et al. (2009) and references therein for details of their respective data reduction procedures.

Once downloaded from their respective databases, spectra underwent some additional reduction procedures. All spectra were corrected for interstellar reddening using NASA/IPAC Infrared Sci-

ence Archive's Galactic Dust Reddening and Extinction Service[1]. Most also showed significant [FeII] absorption, which can contaminate emission line fluxes. Graduate student Amanda Schilling fitted these spectra with [FeII] templates to correct for this effect.

A number of scaling relations can be found in the literature that correlate the spectroscopic properties of an AGN with the mass of its central engine. Many of these are based on reverberation mapping of the broad line region, where the observed Doppler-broadened emission lines originate. The motions of gas and dust in the BLR are thought to be described by the virial equation

$$M_{BH} = \frac{f R \Delta V^2}{G}$$

with BLR radius R, line width ΔV, and scale factor f.

Several studies have found a power-law relationship between R and AGN continuum luminosity L, meaning central black hole mass can be measured from single-epoch observations of AGN, as opposed to the weeks-long observational campaigns required by reverberation mapping proper. This can then be further simplified using the luminosity of a particular wavelength or emission line as a proxy for L. For further details on reverberation mapping and scaling relations, see Peterson & Horne (2004), Vestergaard & Peterson (2006), McLure & Jarvis (2002), and Peterson et al. (2004).

I used the scaling relations of Vestergaard & Peterson (2006) (their equation 6) and McLure & Jarvis (2002) (their equation 7) to determine the mass of each galaxy's central SMBH from the properties of the Hβ and MgII broad emission lines, which trace the motion of the BLR gas. These equations are

$$\log M_{BH}(\mathrm{H}\beta) = \log\left\{\left[\frac{\mathrm{FWHM}(\mathrm{H}\beta)}{1000\ \mathrm{km\ s^{-1}}}\right]^2 \left[\frac{L(\mathrm{H}\beta)}{10^{42}\ \mathrm{ergs\ s^{-1}}}\right]^{0.63}\right\} + (6.67 \pm 0.03) \qquad (2)$$

and

$$\frac{M_{BH}}{M_\odot} = 3.37 \left(\frac{\lambda L_{3000}}{10^{37}\ \mathrm{W}}\right)^{0.47} \left[\frac{\mathrm{FWHM(MgII)}}{\mathrm{km\ s^{-1}}}\right]^2 \qquad (3)$$

respectively. A few AGN in my sample also showed prominent Hα, Hγ, and/or CIV lines in their spectra. Although scaling relations for the first and last of these additional lines are present in the literature (e.g., Greene & Ho 2005 and Vestergaard & Peterson 2006), I focused primarily on Hβ and MgII due to time constraints.

I used the IRAF task `specfit` to model each spectrum, including a power law component to account for the underlying continuum (over a wavelength range that covers the emission lines of interest) and one or more Gaussian components to model emission lines. Most fits included multiple Gaussian components in addition to the broad Hβ and MgII lines (to model the [OIII] λ5007,4959 doublet, narrow Hβ component, etc.) to ensure the best overall fit.

Luminosity distances were computed using an online Cosmology Calculator tool[2] (Wright 2006). If an object had multiple spectra with the same measured line, the spectrum with the most reliable fit (and/or the highest S/N) was used to determine SMBH mass. L_{3000} for spectra with a measurable MgII line was estimated from the observed flux at 3000 Å.

[1] http://irsa.ipac.caltech.edu/applications/DUST/
[2] http://www.astro.ucla.edu/ ~wright/CosmoCalc.html

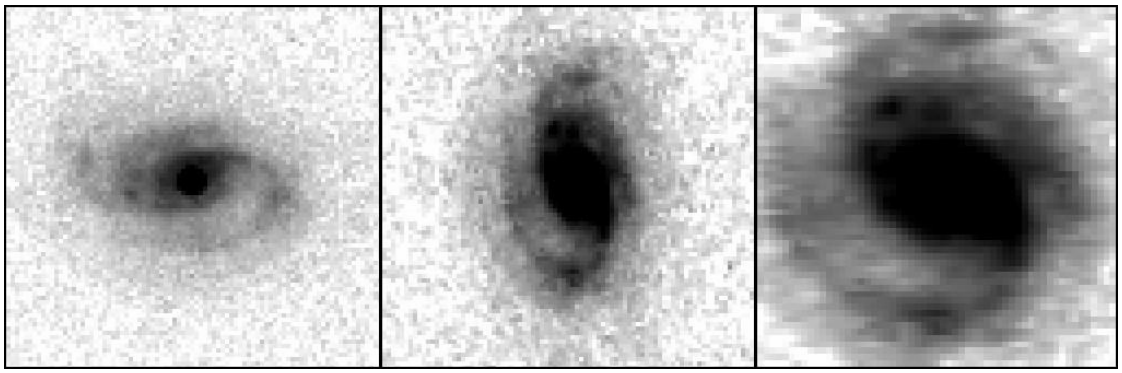

Fig. 2. — Preparing an image of XMMC 61 for pitch angle measurement. *Left*: Galaxy as it appears in the original *HST* image. *Center*: Rotated galaxy, with the isophote semi-major axis aligned vertically. *Right*: Fully deprojected galaxy.

2.2. *Pitch Angle Measurements*

Pitch angles were measured using *I*-band *HST* imaging data with the ACS/WFC F814W filter. Images were retrieved from the Mikulski Archive for Space Telescopes (MAST)[3]. I assume disk galaxies to be intrinsically circular, as observed in face-on spiral galaxies; since disks are generally inclined relative to the observer, forming an ellipsoidal shape on the sky, accurate measurement of pitch angle requires deprojection of the image of the disk. The position angle and apparent ellipticity of each galaxy was determined using the IRAF task `isophote.ellipse`. Each image was then rotated so that the semi-major axis of the ellipse is aligned with the y-axis and magnified in the x-direction, forming the circular disk. Figure 2 shows an example of this process.

Two different techniques were employed to measure pitch angle, which are described briefly here. The first of these involves a two-dimensional fast Fourier transform decomposition, accomplished using the 2DFFT code of Davis et al. (2012). 2DFFT analyzes each image as a superposition of logarithmic spirals within an annulus of fixed outer radius, corresponding to the visible outer edge of the disk, and a variable inner radius r_{inner} (both measured in pixels). The code iterates over all values of r_{inner} from 0 to r_{outer} to determine the dominant harmonic mode m (where $0 < m < 6$) and compute the pitch angle for each mode. The code produces a plot of pitch angle as a function of radius for each mode, where the best-fit pitch manifests itself as a relatively stable value of P over an interval of r. The average pitch over this interval was calculated using a supplementary Python script. Error in the measured pitch angle is calculated by adding in quadrature the quantized error of the 2DFFT code and the standard deviation of P over the interval, weighted by the length of the interval as a fraction of r_{outer}.

The second technique to measure pitch angles is summarized as a variance of means, accomplished using the Spirality code of Shields et al. (2015). Spirality superimposes on the image a series of spiral arm templates consisting of a user-specified number of axes of a certain pitch angle. For an annulus defined by a variable r_{inner} and a fixed r_{outer}, it iterates over a user-specified range of P, computing the mean pixel value along each of the axes for each allowed value of P. Spiral templates whose pitch does not match that of the galaxy's arms produces a low variance, since all axes cross the arms roughly an equal number of times and therefore have roughly the same mean pixel value. However, an axis which exactly traces a real spiral arm has a large pixel value compared to other axes, producing a large variance in the mean pixel value. The best-fit

[3] http://mast.stsci.edu

pitch angle (for a given r_{inner}) is thus recorded as the global maximum in the variance-of-means fitting function. This process is performed over a user-specified range of inner radii, similar to 2DFFT. The overall best-fit pitch is computed as the average of these over all allowed values of r_{inner}. Total error in the measured pitch angle is calculated by adding in quadrature the standard deviation of the overall best-fit pitch angle, weighted by the fractional size of the annulus, and the pitch angle step size.

It should be noted that the values of P reported in table 1 are really the absolute values of the measured pitch angles. Spirals with arms winding counterclockwise are defined to have negative pitch angles, which is merely an orientation effect.

Virtually all fitting functions calculated by Spirality increased monotonically with increasing $|P|$ and showed one or more weak local maxima, typically at $|P| < 20^{\circ}$. I interpret this monotonic increase as a continuum, probably arising from foreground stars or noise in the imaging data, and refined my measurements when possible to focus more directly on the local maxima, which I interpret as real measurements of P.

If the best-fit values of P computed by 2DFFT and Spirality were consistent with each other within their respective error bars, I used their average (and the average of their errors) as the reported pitch angle and error. 2DFFT and Spirality did not, however, have consistent best-fit pitch angles for most galaxies in my sample, though they often agreed on the dominant harmonic mode. For these galaxies I inspected each galaxy image by eye, using a spiral overlay program to determine which result better traces the spiral pattern.

Each method has its respective advantages over the other. Spirality, for example, does not assume a single harmonic mode or particular symmetry in the spiral pattern, though it is more sensitive than 2DFFT to foreground stars which can contaminate the fitting function. Spirality also assumes purely logarithmic structure across a galaxy within the measurement annulus, while 2DFFT only assumes that the observed patterns can be described as a superposition of logarithmic spirals. Some evidence suggests that spiral galaxies are indeed not strictly logarithmic across the entire disk. In particular, Savchenko & Reshetnikov (2013) report a small but noticeable shift towards smaller absolute pitch angles – a tightening of the spiral arms – as the inner radius of the measurement annulus increases. This can loosely be interpreted in Newtonian terms as an effect of the mass enclosed at some radius r: as enclosed mass increases in the inner part of the disk, the stars and gas on the outer edges will be subject to a greater gravitational attraction, pulling the spiral arms in.

New evidence also suggests that measured pitch angle depends on the waveband of the image used for the measurement, though the typical difference across wavebands is, at most, approximately 5 degrees (Pour Imani et al. in prep.). This is consistent with the density wave theory of spiral morphology, which predicts slight differences in the pitch angle across wavebands due to shearing effects. This contradicts previous findings like those of Davis et al. (2012), who found little or no dependence of pitch angle on the observation wavelength. Although this potential new effect must be taken into consideration when analyzing the combined M-P relation (to be done in future work), the uniformity of my imaging data, together with the fact that differences in pitch angle across wavebands are small at best, means this phenomenon can be safely ignored for the purposes of this paper.

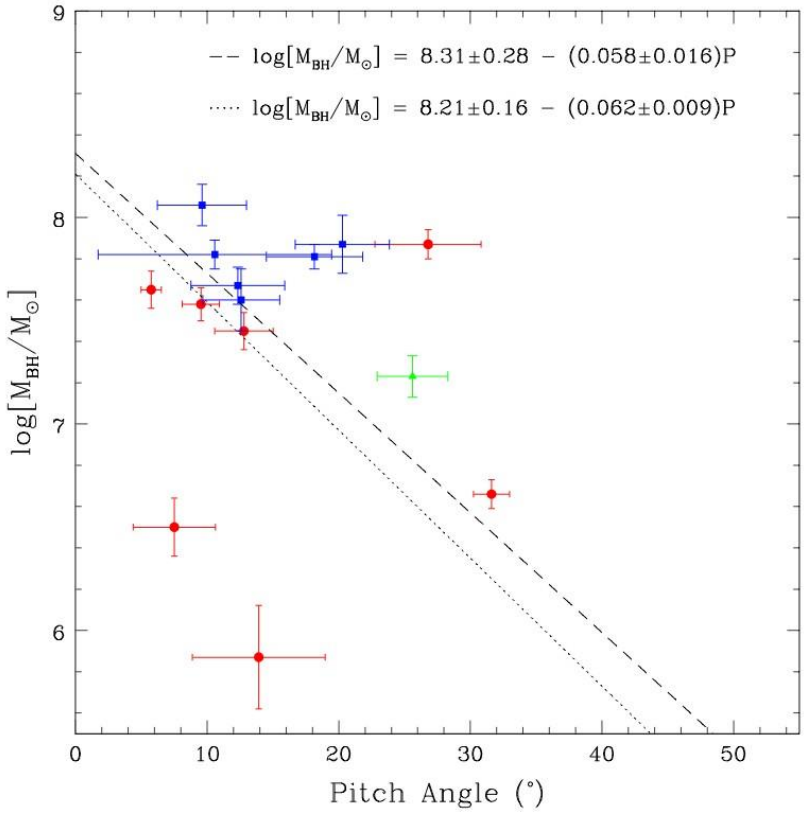

Fig. 3. — SMBH mass vs. spiral arm pitch angle for all galaxies in my sample. Red circles indicate mass estimates from H*β*; blue squares indicate mass estimates from MgII; and the green triangle indicates a mixed mass estimate. The dashed line is the best fit to the data; the dotted line is the *M-P* relation of Berrier et al.

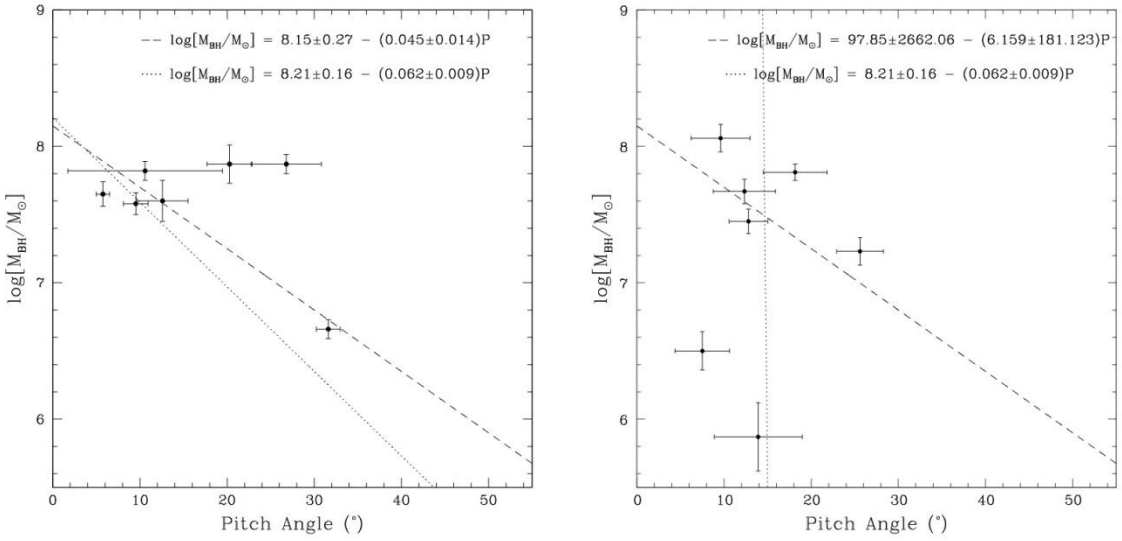

Fig. 4. — *Left*: SMBH mass vs. pitch angle for strongly barred spiral galaxies. *Right*: SMBH mass vs. pitch angle for galaxies which are at most weakly barred.

3. RESULTS

The best-fit line for the points plotted in figure 3 was computed using orthogonal distance regression. The best-fit relation for the full sample is

$$\log(M/M_{\odot}) = (8.31 \pm 0.28) - (0.058 \pm 0.016)P. \quad (4)$$

This fit has a residual variance of 9.155 and a scatter of 0.74 dex. This is almost identical to the *M-P* relation of Berrier et al. (2013), which is shown in the same plot for comparison. Orthogonal distance regression, also known as Deming regression, was chosen over a weighted least-squares fit to account for the errors in both variables. I also separated these galaxies by eye into weakly barred/unbarred and strongly barred subsamples. Figure 4 shows data points and the best-fit equation for each of these groups, again with the *M-P* relation of Berrier et al. (2013) for comparison.

It should be noted that the Hβ line for XMMC 2234 was relatively narrow and weak, with a FWHM of approximately 850 km s^{-1} and a small flux compared to the neighboring [OIII] λ5007,4959 doublet. The weakness of the broad Hβ line, together with the high inclination of the disk in the original *HST* image, may suggest some obscuration of the BLR emission. If this is the case, the value of M_{BH} reported in this work should be interpreted as a lower limit on black hole mass for XMMC 2234; whether or not this really is the case remains open for investigation. Removing this object from the sample does not significantly affect the fit or its scatter.

4. DISCUSSION

Although the best-fit *M-P* relation for my total sample is virtually identical to that of Berrier et al. (2013), the fit for the barred subsample is considerably shallower. This could suggest some evolution in the slope of the *M-P* relation with increasing redshift, which may be interpreted as a systematic shift towards higher-mass SMBHs compared to their low-*z* counterparts at a given pitch angle. With only seven data points, this conclusion is largely tentative, but is bolstered when considering the combined type 1 AGN sample of all contributors to the *M-P* relation project. Figure 5 shows data for all type 1 AGNs in the combined sample as of October 2015. This plot, which more strongly suggests evolution in the *M-P* relation with redshift, includes a portion of the sample reported here, as well as $z > 0.04$ galaxies analyzed by A. Schilling and A. Hughes.

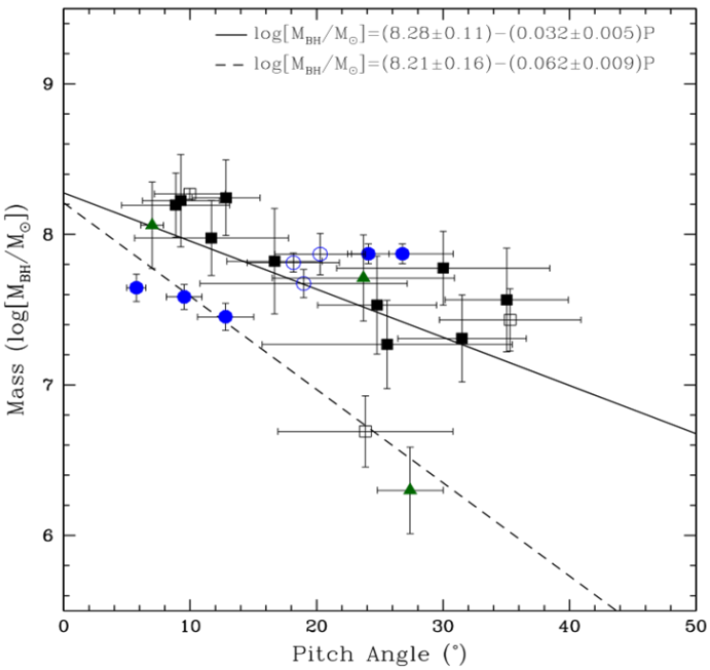

Fig. 5. — SMBH mass vs. spiral arm pitch angle for the combined sample. Open circles indicate mass estimates from CIV; triangles indicate MgII; and all other points indicate Hβ. The solid line is a weighted least squares fit; the dashed line is the *M-P* relation of Berrier et al. (2013). Graph created by A. Schilling.

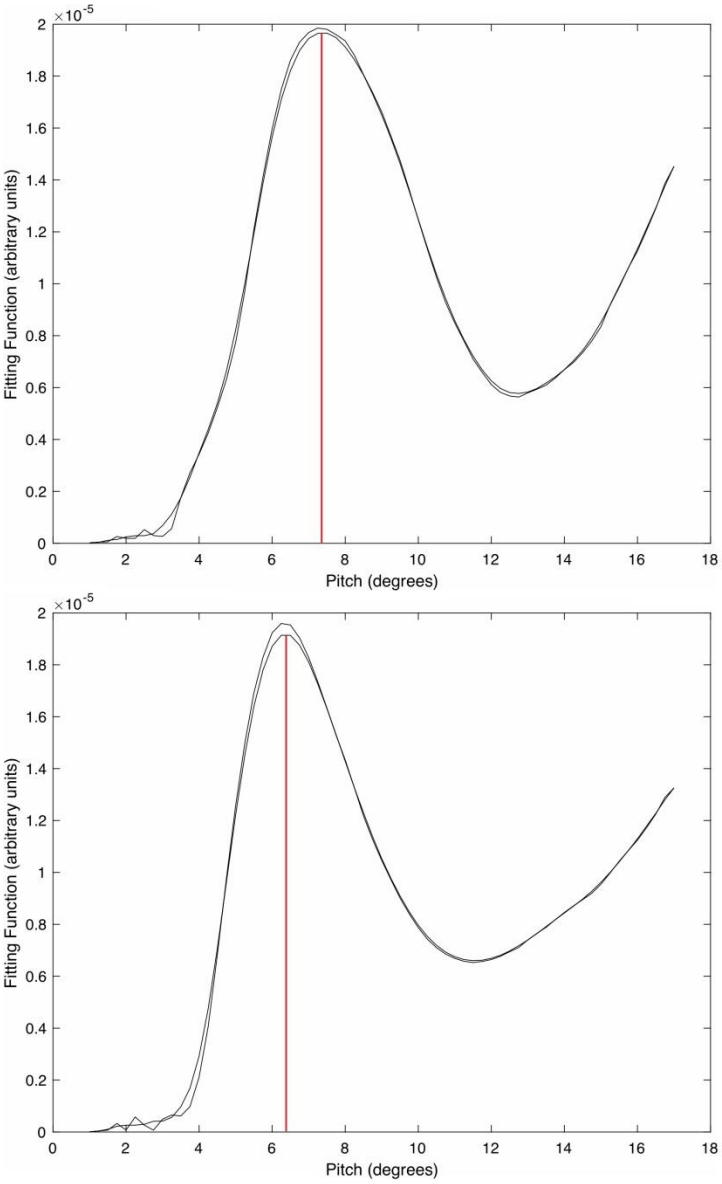

Fig. 6. — Spirality outputs for XMMC 56. The maximum in the fitting function occurs at approximately 7.25 deg. when r_{inner} = 5.5 pixels (top) and at 6.25 deg. when r_{inner} = 6.5 pixels (bottom).

Plots produced by Spirality for seven galaxies showed evidence of decreasing $|P|$ with increasing inner radius, consistent with the results of Savchenko & Reshetnikov (2013). Figure 6 shows an example of this effect in XMMC 56, which occurs over most inner radii where the maxima in the fitting function are well-defined; even an increase in the value of r_{inner} of one pixel produces a clear drift in the maximum. However, a similar trend was apparent only in the 2DFFT data for 2-4 of these seven galaxies. Whether this effect is real and quantifiable or simply a quirk of the Spirality and 2DFFT codes remains an open question to be addressed in future work. Other possible avenues for further inquiry include the corroboration of black hole mass measurements using the M-σ_* relation and the application of a newly-developed fundamental plane relation for disk galaxies (Davis et al. 2015). Greene & Ho (2005) showed that the FWHM of the core of the [OIII] λ5007 emission line can be used to estimate the velocity dispersion of the bulge gas σ_g. This can then be used as a proxy for the bulge stellar velocity dispersion in the M-σ_* relation, providing an independent estimate of the mass of the nuclear black hole in galaxies where [OIII] λ5007 emission is observed. In addition, Davis et al. (2015) recently formulated a planar relationship between the tangent of a spiral galaxy's pitch angle $\tan|P|$, the stellar mass of its bulge, and the density of neutral hydrogen in the disk of the galaxy. It will be worth investigating whether any archival data exists for galaxies in my sample from which the gas densities may be inferred. In particular, the two lowest-mass galaxies shown in Figure 3 appear to be extreme deviations from an otherwise linear relationship, with rather undermassive black holes for their measured pitch angles. Observations of the gas densities in these outlier galaxies would provide evidence on whether they occupy a significantly different "slice" of the fundamental plane of Davis et al. (2015), compared to the rest of my sample.

I would like to acknowledge the Arkansas Center for Space and Planetary Sciences Research Experience for Undergraduates, which is funded by the National Science Foundation, for supporting a portion of this work (AST-1157002).

This work has made use of data from SDSS Data Releases 7, 9, and 12. Funding for SDSS-III has been provided by the Alfred P. Sloan Foundation, the Participating Institutions, the National Science Foundation, and the U.S. Department of Energy Office of Science. The SDSS-III web site is http://www.sdss3.org/. SDSS-III is managed by the Astrophysical Research Consortium for the Participating Institutions of the SDSS-III Collaboration including the University of Arizona, the Brazilian Participation Group, Brookhaven National Laboratory, Carnegie Mellon University, University of Florida, the French Participation Group, the German Participation Group, Harvard University, the Instituto de Astrofisica de Canarias, the Michigan State/Notre Dame/JINA Participation Group, Johns Hopkins University, Lawrence Berkeley National Laboratory, Max Planck Institute for Astrophysics, Max Planck Institute for Extraterrestrial Physics, New Mexico State University, New York University, Ohio State University, Pennsylvania State University, University of Portsmouth, Princeton University, the Spanish Participation Group, University of Tokyo, University of Utah, Vanderbilt University, University of Virginia, University of Washington, and Yale University. Some data presented in this paper were obtained from the Mikulski Archive for Space Telescopes (MAST). STScI is operated by the Association of Universities for Research in Astronomy, Inc., under NASA contract NAS5-26555. Support for MAST for non-*HST* data is provided by the NASA Office of Space Science via grant NNX09AF08G and by other grants and contracts.

REFERENCES

Alam, S. et al. 2015. ApJS, 219, 12.
Antonucci, R. 1993. ARA&A, 31, 473.
Bennett, C. L., Larson, D., Weiland, J. L., & Hinshaw, G. 2014. ApJ, 794, 135.
Berrier, J. C., et al. 2013. ApJ, 769, 312.
Davis, B. L., Berrier, J. C., Shields, D. W., Kennefick, J., Kennefick, D., Seigar, M. S., Lacy, C. H. S., & Puerari, I. 2012. ApJS, 199, 33.
Davis, B. L. et al. 2014. ApJ, 789, 124.
Davis, B. L. et al. 2015. ApJL, 802, L13.
Ferrarese, L. & Ford, H. 2005. SSRv, 116, 523.
Ferrarese, L. & Merritt, D. 2000. ApJL, 539, L9.
Gebhardt, K. et al. 2000. ApJL, 539, L13.
Graham, A. W. & Driver, S. P. 2007. ApJ, 655, 77
Graham, A. W. 2016. ASSL, 418, 263.
Greene, J. E. & Ho, L. C. 2005. ApJ, 627, 721.
Greene, J. E. & Ho, L. C. 2005. ApJ, 630, 122.
Kazanas, D., Fukumara, K., Behar, E., Contopoulos, I., & Shrader, C. 2012. Ast. Rev., 7, 92.
Kormendy, J. & Gebhardt, K. 2001. AIP Conf. Proc. 586, 20th Texas Symposium on relativistic astrophysics, ed. Wheeler, J. C. & Martel, H., 363.
Lilly, S. J. et al. 2007. ApJS, 172, 70.
Lin, C. C. & Shu, F. H. 1964. ApJ, 140, 646.
Lusso, E. et al. 2010. A&A, 512, A34.
Lynden-Bell, D. 1969. Nature, 223, 690.
Lynden-Bell, D. & Rees, M. MNRAS, 152, 461.
Magorrian, J., et al. 1998. AJ, 115, 2285.
McLure, R. J. & Jarvis, M. J. 2002. MNRAS, 337, 109.
Peterson, B. M. & Horne, K. 2004. "Planets to Cosmology: Essential Science in Hubble's Final Years," Proceedings of the Space Telescope Science Institute Symposium, ed. Livio, M.
Peterson, B. M. et al. 2004. ApJ, 613, 682.
Pour Imani, H. et al. In preparation.
Prescott, M. K. M., Impey, C. D., Cool, R. J., & Scoville, N. Z. 2006. ApJ, 644, 100.
Rees, M. 1984. ARA&A, 22, 471.
Romero-Gómez, M., Masdemont, J. J., Athanassoula, E., & García-Gómez, C. A&A, 453, 39.
Savchenko, S. S. & Reshetnikov, V. P. 2013. MNRAS, 436, 1074.
Seigar, M. S., Kennefick, D., Kennefick, J., & Lacy, C. H. S. 2008. ApJL, 678, L93.
Shields, D. W. et al. 2015, submitted.
Shu, F. H. 1984. IAU Colloq. 75: Planetary Rings, ed. Greenberg, R. & Brahic, A. 513.
Trump, J. R. et al. 2009. ApJ, 696, 1195.
Urry, M. C. & Padovani, P. 1995. PASP, 107, 803.
Vestergaard, M. & Peterson, B. M. 2006. ApJ, 641, 689.
Woo, J. et al. 2013. ApJ, 772, 49.
Wright, E. L. 2006. PASP, 118, 1711.